# Particle acceleration and magnetic field amplification in the jets of 4C74.26

A.T. Araudo[1], A.R. Bell[2] and K.M. Blundell[1]

## ABSTRACT

We model the multi-wavelength emission in the southern hotspot of the radio quasar 4C74.26. The synchrotron radio emission is resolved near the shock with the MERLIN radio-interferometer, and the rapid decay of this emission behind the shock is interpreted as the decay of the amplified downstream magnetic field as expected for small scale turbulence. Electrons are accelerated to only 0.3 TeV, consistent with a diffusion coefficient many orders of magnitude greater than in the Bohm regime. If the same diffusion coefficient applies to the protons, their maximum energy is only $\sim 100$ TeV.

*Subject headings:* galaxies: active — galaxies: jets — quasars: individual(4C74.26) — acceleration of particles — radiation mechanisms: non-thermal — shock waves

## 1. Introduction

Diffusive shock acceleration (DSA) is an established mechanism to convert bulk kinetic energy into a non-thermal distribution of relativistic particles with a maximum energy much larger than the average energy of particles in the plasma. This theory explains well the spectrum of Galactic cosmic rays (CR) with energies up to $\sim$3 PeV, accelerated in supernova remnant shocks (see Bell 2014, for a review). The most energetic CR, i.e. particles with energies up to 50 EeV, are accelerated outside the Galaxy but the origin of these particles is still unknown. Relativistic shocks in extragalactic sources like Gamma Ray Bursts and Active Galactic Nuclei have been proposed as candidates (e.g. Gallant & Achterberg 1999; Murase et al. 2012). However, theoretical models (Pelletier et al. 2009; Lemoine & Pelletier 2010; Sironi et al. 2013; Reville & Bell 2014) show magnetic field amplification at ultra-relativistic shocks on scales much smaller than the Larmor radius $r_{\rm g}$ of particles being accelerated which precludes CR acceleration to EeV energies unless other processes can be found to amplify the magnetic field on larger scales.

Hotspots are usually detected at the jet termination region in type II Fanaroff-Riley (FR) radiogalaxies (Fanaroff & Riley 1974). The location of the hotspot is coincident with the downstream region of the jet termination shock, where particles accelerated by the shock emit synchrotron radiation. Therefore, hotspots are suitable places to study DSA in high velocity shocks.

We model the emission from radio to X-rays in the southern hotspot of the FR II source 4C74.26 using data provided in Erlund et al. (2010). We determine that the compact radio emission traces out the location of the shock where the magnetic field $B$ is amplified by plasma instabilities up to $\sim$100 $\mu$G, and it damps rapidly downstream of the shock. The turnover in the synchrotron spectrum between infrared (IR) and optical wavelengths implies that the CR electron scattering length is much longer than the Larmor radius and consistent with the amplified magnetic field being structured on very small scales and comparable with the ion skin-depth $c/\omega_{\rm pi}$. Cosmic ray acceleration is consequently very slow and electrons are accelerated to only $E_{e,\rm max} \sim 0.3$ TeV. A similarly low acceleration rate for ions would limit their energy to $\sim 100$ TeV and preclude proton acceleration to

[1]University of Oxford, Astrophysics, Keble Road, Oxford OX1 3RH, UK

[2]University of Oxford, Clarendon Laboratory, Parks Road, Oxford OX1 3PU, UK

EeV energies.

## 2. The giant FR II galaxy 4C74.26

The FR II galaxy 4C74.26 is located at redshift $z = 0.104$ ($\sim$0.5 Gpc from Earth)[1]. Two X-ray sources separated by $\sim 10''$ were detected with Chandra (by Erlund et al. 2010) at the termination region of the southern jet, as shown in Figure 1 (upper). In the present work we study the southern X-ray source, with a luminosity $L_{\rm x} \sim 10^{41}$ erg s$^{-1}$ at 2 keV and called "the southern arc". The shape of this emission is arc-like with a characteristic size $l_{\rm x} \sim 10''$, and encloses a compact radio source.

### 2.1. The southern arc

Compact radio emission from the southern arc was detected with the MERLIN high resolution interferometer ($\nu_{\rm r} = 1.66$ GHz) with a flux $f_{\rm r} \sim$0.04 Jy, and luminosity $L_{\rm r} \sim 1.9{\times}10^{40}$ erg s$^{-1}$ per unit logarithmic bandwidth $\delta\nu = \nu$. This emission is located in a region of width $l_{\rm r} < 1''$ on the plane of the sky. In addition, faint and diffuse radiation was detected at IR ($\nu_{\rm ir} = 1.36{\times}10^{14}$ Hz) and optical ($\nu_{\rm opt} = 6.3{\times}10^{14}$ Hz) bands, with fluxes $\sim 8.4{\times}10^{-6}$ and $2.82{\times}10^{-7}$ Jy, respectively, and located in a region of width $\gtrsim l_{\rm r}$. However, there is a linear structure (in both bands) that traces the brightest edge of the MERLIN radio emission, and seems to be cupped within it.

Two factors indicate that the southern arc of X-ray emission is not synchrotron. First, $l_{\rm x} > l_{\rm r}$ is inconsistent with the X-ray emitting electrons being more energetic and therefore cooling more rapidly as they advect away from the shock. Second, the steep spectrum between IR and optical (see Fig. 13 in Erlund et al. 2010) indicates the maximum energy of (synchrotron) emitting electrons. We note that similar characteristics are observed in other sources (e.g. Orienti et al. 2012).

Erlund et al. (2010) suggested that the multiwavelength emission from the southern arc is produced by non-thermal electrons, emitting synchrotron radiation from radio to optical, and up-scattering the cosmic microwave background

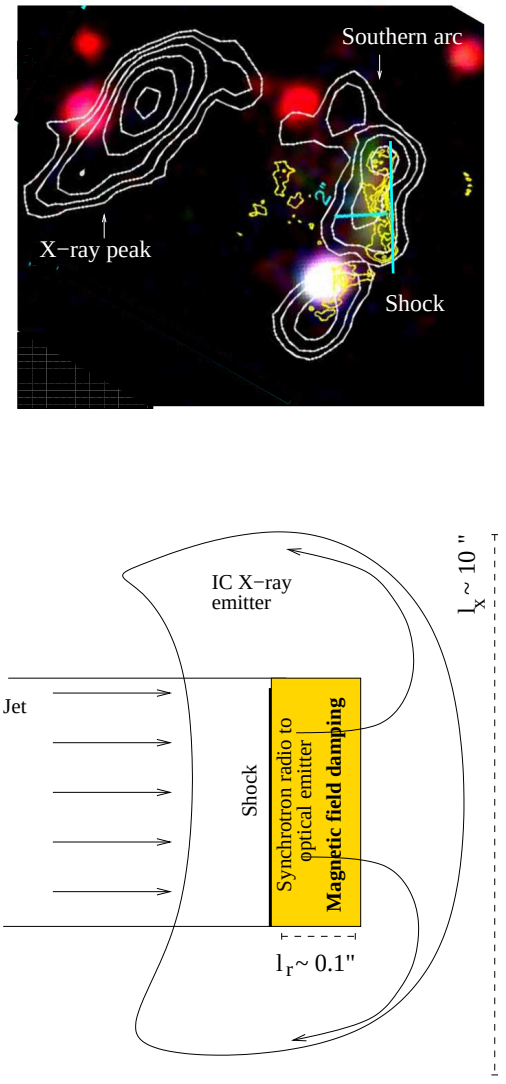


Fig. 1.— *Upper:* the hotspot(s) at the southern jet of the FR II galaxy 4C74.26 (adapted and rotated by $\sim 60°$ from Erlund et al. 2010). White and yellow contours are X-rays and radio data, respectively. Red and green correspond to IR and optical, respectively. *Lower:* sketch of our model of the southern arc (not to scale). The synchrotron radio-to-optical radiation is located within the compact MERLIN emitter, whereas IC X-ray emission is produced in a more extended region.

[1]Throughout this paper we use the cosmology $H_0 = 71$ km s$^{-1}$ Mpc$^{-1}$, $\Omega_0 = 1$ and $\Lambda_0 = 0.73$. One arcsecond represents1.887 kpc on the plane of the sky at $z = 0.104$.

(CMB) photons (with energy $\sim 7\times10^{-4}$ eV and energy density $U_{\rm cmb}$ $=6\times10^{-13}$ erg cm$^{-3}$) to the X-ray domain. In this scenario, the radio-to-IR spectral index is $\alpha = 0.75$ (the synchrotron flux density at frequency $\nu$ is $f_\nu \propto \nu^{-\alpha}$), which corresponds to $p = 2.5$ in the non-thermal electron energy distribution when the emission is produced in the same volume.

## 3. The hotspot as a magnetic field damping region

In this work we consider the same emission mechanisms as in Erlund et al. (2010), but allow the synchrotron and Inverse Compton (IC) emission to be produced in regions with different spatial extents. In particular; electrons accelerated at the shock emit synchrotron radiation from radio to optical in a compact region behind the shock, whereas the IC X-ray emission is located in an extended region. In Fig. 1 (lower) we sketch our model.

The synchrotron (s) and IC cooling length of electrons with Lorentz factor $\gamma$ is $l_{\rm s,ic}(\gamma) = t_{\rm s,ic}(\gamma)v_{\rm sh}/r$, where $t_{\rm s,ic}(\gamma)$ is the cooling timescale. The shock velocity is approximately the same as the jet velocity which we take characteristically to be $v_{\rm sh} = 10^{10}$ cm s$^{-1}$ ($\sim c/3$ and Lorentz factor $\Gamma_{\rm sh} \sim 1.06$) in line with observations of similar objects (see Steenbrugge & Blundell 2008, and references therein). We use $r = 7$ as the shock compression ratio for a non-relativistic shock whose downstream thermal pressure is dominated by relativistic electrons, although $r \sim 4$ may still apply if non-relativistic ions dominate the pressure downstream of the shock (Kirk et al. 2000). Our conclusions are not sensitive to the exact value of $r$.

### 3.1. Inverse Compton X-ray emission

The IC X-ray emission is produced by electrons with $\gamma_{\rm x} \sim 10^3$ and $l_{\rm ic}(\gamma_{\rm x}) \sim 10^4(v_{\rm sh}/10^{10}\,{\rm cm\,s^{-1}})$ arcsec, which is much larger than $l_{\rm x}$. The synchrotron cooling length $l_{\rm s}(\gamma_{\rm x})$ is also greater than $l_{\rm x}$, unless the magnetic field in the X-ray emitting region is $\sim$ 360 $\mu$G. However, such a large magnetic field would produce synchrotron radio radio emission much brighter than $L_{\rm r}$ (see next section). Furthermore, we show below that the amplified magnetic field, of the order of $\sim$100 $\mu$G, is confined to a small volume close to the shock. Therefore, adiabatic expansion is probably the dominant cooling mechanism as the particles flow out of the hotspot.

Unless $\Gamma_{\rm sh} \gtrsim 10$, X-ray emitting electrons are non-thermal and follow a power law energy distribution $\propto \gamma^{-p}$ (e.g. Giannios & Spitkovsky 2009). Assuming that the X-ray emitting volume is $V_{\rm x} \sim 300$ arcsec$^3$, the energy density of these non-thermal electrons is $\sim 10^{-9}(\gamma_{\rm min}/50)^{-0.5}$ erg cm$^{-3}$ where the power law terminates at a minimum Lorentz factor $\gamma_{\rm min}$. The magnetic field with the same energy density is $\sim 100(\gamma_{\rm min}/50)^{-0.25}$ $\mu$G. These results correspond to the case where $p = 2.5$ (see however Sect. 3.2.2). In the following sections we take 100 $\mu$G as a fiducial magnetic field since it represents equipartition between magnetic and relativistic electron energy densities and is typical of other hotspots (e.g. Godfrey & Shabala 2013).

### 3.2. Synchrotron emission

Considering that $\gamma(\nu) \sim 4.5 \times 10^{-4}(\nu/B)^{0.5}$ is the Lorentz factor of electrons emitting synchrotron radiation at $\nu$ in a magnetic field $B$, $l_{\rm s}$ can be written as

$$\frac{l_{\rm s}(\nu)}{[\prime\prime]} \sim 12 \left(\frac{\nu}{\rm GHz}\right)^{-0.5} \left(\frac{B}{100\,\mu{\rm G}}\right)^{-1.5} \left(\frac{v_{\rm sh}}{10^{10}\,{\rm cm\,s^{-1}}}\right). \quad (1)$$

#### *3.2.1. Radio*

MERLIN emitting electrons have $\gamma_{\rm r} \equiv \gamma(\nu_{\rm r}) \sim 2\gamma_{\rm x}(B/100\,\mu{\rm G})^{-0.5}$. If both radio and X-ray emission are produced by non-thermal electrons that follow the same power-law energy distribution, $L_{\rm x}/L_{\rm r} \sim (\gamma_{\rm x}/\gamma_{\rm r})^{3-p}(U_{\rm cmb}/U_{\rm mag})V_{\rm x}/V_{\rm r}$ and $B \sim 100$ $\mu$G corresponds to $V_{\rm x}/V_{\rm r} \sim 5 \times 10^3$, where $U_{\rm mag} = B^2/8\pi$ and $V_{\rm r}$ is the volume of the synchrotron emitter[2]. Such a large ratio between emitting volumes is not implausible provided the magnetic field is inhomogeneous in the shock downstream region and the synchrotron emitter consists of features smaller than the MERLIN point spread function (FWHM $0.15''$) as seen in parts of the MERLIN data.

The synchrotron cooling length of MERLIN emitting electrons is $l_{\rm s}(\nu_{\rm r}) \sim 9.3''(B/100\,\mu{\rm G})^{-3/2}(v_{\rm sh}/10^{10}\,{\rm cm\,s^{-1}})$, and a very large magnetic field of $\sim 2.4\,(v_{\rm sh}/10^{10}\,{\rm cm\,s^{-1}})^{2/3}$ mG

[2]Note that if $V_{\rm x} = V_{\rm r}$, an unrealistically small magnetic field of 0.3 $\mu$G would be needed to explain the observed fluxes.

would be required to match $l_{\rm s}(\nu_{\rm r}) = 0.1'' \sim l_{\rm r}$. This result suggests that the downstream extent of the compact emission detected at $\nu_{\rm r}$ is not the result of fast synchrotron cooling, as we can confirm when we take into account the IR emission.

### *3.2.2. Infrared*

The synchrotron cooling length of IR emitting electrons is $l_{\rm s}(\nu_{\rm ir}) \sim 0.03''(B/100\,\mu{\rm G})^{-3/2}(v_{\rm sh}/10^{10}\,{\rm cm\,s^{-1}})$, indicating that these particles radiate most of their energy within $l_{\rm r}$. (This angular distance is not resolved by the IR observations.) This is consistent with a radio-to-IR electron energy spectral index of $p \sim 2.5$ with the cooling break in the spectrum occuring close to IR wavelengths[3]. Note that if the emitting volume were determined by synchrotron cooling, $l_{\rm s}(\nu) \propto \nu^{-0.5}$ giving $p = 2\alpha = 1.5$ since $\alpha$ is measured to be 0.75. This very hard spectrum is unlikely since it diverges toward high energy and would be remarkable in hotspots, supporting the conclusion that the downstream radio extent $l_{\rm r}$ must be determined by factors other than synchrotron cooling. As we discuss in Sect. 4 this may be the result of the damping of the magnetic field (see Schure et al. 2012, for a review).

### *3.2.3. Optical*

Optical emission produced by synchrotron radiation of electrons with $\gamma(\nu_{\rm opt}) \sim \gamma(\nu_{\rm ir})$ is almost co-spatial with the IR emission, and this explains the linear structure cupped within $l_{\rm r}$[4]. The synchrotron turnover $\nu_{\rm c}$ between $\nu_{\rm ir}$ and $\nu_{\rm opt}$ indicates that the maximum energy of non-thermal electrons is $E_{e,\rm max} \sim \gamma(\nu_{\rm c})m_e c^2 \sim 0.3(\nu_{\rm c}/\nu_{\rm ir})^{0.5}(B/100\mu{\rm G})^{-0.5}$ TeV.

## 4. Magnetic field amplification

The amplification of the magnetic field at strong shocks in supernova remnants was demonstrated by Vink & Laming (2003) and Berezhko et al. (2003), deriving the magnetic field from $l_{\rm s}$ downstream of the shock. A theoretical explanation was provided by Bell (2004) showing that non-resonant hybrid instabilities are capable of enhancing the magnetic field by orders of magnitude. Magnetic field amplification is also responsible for $B \sim 100$ $\mu$G in the southern arc in 4C74.26 since it is much larger than the expected value in the jet upstream of the termination shock (e.g. Hardcastle & Krause 2014).

Bohm diffusion (electron mean free path $\lambda \sim r_{\rm g}$) in a $\sim$100 $\mu$G magnetic field would be expected to accelerate electrons with synchrotron X-ray emitting energies as seen in supernova remnants (Stage et al. 2006). However, $\nu_{\rm c} \sim \nu_{\rm ir,opt}$ determined by a competition between shock acceleration and synchrotron cooling indicates that acceleration is slow and therefore that the electron diffusion coefficient $D$ is much larger than the Bohm value $D_{\rm Bohm}$:

$$\frac{D}{D_{\rm Bohm}} \sim 10^6 \left(\frac{v_{\rm sh}}{10^{10}\,{\rm cm\,s^{-1}}}\right)^2 \left(\frac{\nu_{\rm ir}}{\nu_{\rm c}}\right), \quad (2)$$

independent of $B$ (see e.g. Casse et al. 2002). Such a large diffusion coefficient in an amplified magnetic field is expected if it is structured on a scale $s$ much smaller than the Larmor radius of the electrons being accelerated. Small angle scattering by magnetic field randomly orientated in cells of size $s$ produces $D \sim (r_{\rm g}/s)D_{\rm Bohm}$ and then

$$\frac{s}{\rm cm} \sim 10^7 \left(\frac{\nu_{\rm c}}{\nu_{\rm ir}}\right)^{1.5} \left(\frac{B}{100\,\mu{\rm G}}\right)^{-1.5} \left(\frac{v_{\rm sh}}{10^{10}\,{\rm cm\,s^{-1}}}\right)^{-2}. \quad (3)$$

In comparison the ion skin-depth is $c/\omega_{\rm pi} \sim 2.3 \times 10^9\,(n/10^{-4}\,{\rm cm^{-3}})^{-0.5}$ cm, where $n$ is the particle density downstream of the shock (assumed to be 7 times the jet density), and

$$\frac{s}{c/\omega_{\rm pi}} \sim \quad 0.01 \left(\frac{\nu_{\rm c}}{\nu_{\rm ir}}\right)^{1.5} \left(\frac{v_{\rm sh}}{10^{10}\,{\rm cm\,s^{-1}}}\right)^{-2} \left(\frac{B}{100\,\mu{\rm G}}\right)^{-1.5} \left(\frac{n}{10^{-4}\,{\rm cm^{-3}}}\right)^{0.5}. \quad (4)$$

Given the uncertainties in the parameter values, the approximate nature of the theoretical models, and the wide range of the spatial scales ($s$, $r_{\rm g}$, $l_{\rm r}$), it is not significant or surprising that our estimate of $s/(c/\omega_{\rm pi})$ differs from unity by a factor of $\sim 0.01$. The order of magnitude similarity of $s$ and $c/\omega_{\rm pi}$ supports the contention that shock-generated small-scale turbulence scatters non-thermal electrons during diffusive shock acceleration. This is consistent with

[3] Note that the relationship $p = (r+2)/(r-1)$ breaks down for mildly relativistic shocks (Kirk et al. 2000; Bell et al. 2011) or when non-linear feedback is important (e.g. Amato & Blasi 2005).

[4] The faint diffuse IR and optical emission may be the result of CMB photons up-scattered by electrons with $\gamma \sim 50$.

Sironi & Spitkovsky (2011) who discuss the various processes related to the Weibel instability that excite turbulence on the characteristic scale of $c/\omega_{\rm pi}$. Simulations show that magnetic field generated by the Weibel instability decays downstream of the shock because of its relatively small scalelength (Sironi & Spitkovsky 2011; Bret et al. 2013; Sironi et al. 2013). This would account for the cut-off of synchrotron emission in 4C74.26 far short of the synchrotron cooling distance of radio-emitting electrons ($l_{\rm r} \ll l_{\rm s}(\nu_{\rm r})$). These electrons continue up-scattering CMB photons, thus producing IC X-ray emission downstream of the shock after the MERLIN radio emission has ceased.

### 4.1. Limit on ions maximum energy

Since the response of highly relativistic ions is similar to that of electrons with the same energy in a tangled amplified magnetic field, we can expect protons to have a similar ratio of $D/D_{\rm Bohm}$. Protons can be accelerated to higher energies than electrons because their radiative losses are minimal, but the maximum energy to which they are accelerated is limited because their acceleration time is increased by the ratio $D/D_{\rm Bohm}$. The Hillas parameter $v_{\rm sh}\,B\,R$ (Hillas 1984), where $R \sim 2''$ ($\sim 2.8$ kpc) is the characteristic length of the source, would suggest proton acceleration to $\sim$100 EeV in the termination shock of 4C74.26, but the maximum energy is reduced to only $\sim$100 TeV if $D \sim 10^6\,D_{\rm Bohm}$ since the Hillas parameter assumes $D \sim D_{\rm Bohm}$ and is otherwise reduced by the factor $(D/D_{\rm Bohm})^{-1}$. Another perspective on the same effect is that the mean free path for scattering by small-scale turbulence $\lambda \sim r_{\rm g}^2/s$ is larger than the size of the system if $s \sim c/\omega_{\rm pi}$ and $r_{\rm g}$ is the Larmor radius of an EeV proton. This result suggests that the mildly relativistic termination shock in 4C74.26 is a poor accelerator of UHECR.

## 5. Conclusions

We model the radio to X-ray emission in the southern hotspot of the FR II galaxy 4C74.26. Our study is based on three key observational features: 1) Compact MERLIN emission region: it is too thin to be the result of fast synchrotron cooling (Sect. 3.2.1). 2) The radio to IR spectrum ($\alpha = 0.75$) is too flat for the emitting volume to be determined by synchrotron cooling through this wavelength range (Sect. 3.2.2). 3) The turnover of the synchrotron spectrum at IR/optical frequencies requires $\lambda \gg r_{\rm g}$ for any reasonable shock velocity (Sect. 4). These three features fit well in a scenario in which the MERLIN radio emission traces out the region where the magnetic field is amplified by plasma instabilities with small length scale (e.g. Weibel).

The magnetic field in equipartition with non-thermal electrons in the MERLIN emission region is $\sim$100 $\mu$G and similar to the values obtained by other authors (e.g. Godfrey & Shabala 2013). An unrealistically large magnetic field $\sim 2.4\,(v_{\rm sh}/10^{10}\,{\rm cm\,s^{-1}})^{2/3}$ mG would be needed to explain the compact radio emission in terms of synchrotron cooling. If $B \sim 100$ $\mu$G in the synchrotron emission region, the maximum energy of non-thermal electrons is $\sim$0.3 TeV.

If ions are accelerated as well, protons with energy $\sim$0.3 TeV diffuse also with mean free path $\lambda \gg r_{\rm g}$. If $\lambda$ is similarly larger than the Larmor radius at higher proton energies, then the maximum proton energy at the termination shock of 4C74.26 is only 100 TeV instead of the 100 EeV indicated by the Hillas parameter. This may have important implications for the understanding of the origins of UHECR.

We thank the referees for the constructive reports. The research leading to this article has received funding from the European Research Council under the European Community's Seventh Framework Programme (FP7/2007-2013)/ERC grant agreement no. 247039. We acknowledge support from the UK Science and Technology Facilities Council under grant number ST/K00106X/1.

## REFERENCES

Amato, E., & Blasi, P., 2005, MNRAS, 364, L76

Bell, A. 2004, MNRAS, 353, 550

Bell, A., Schure, K., & Reville, B., 2011, MNRAS, 418, 1208

Bell, A. 2014, Braz. J. Phys., 44, 415

Berezhko, E., Ksenofontov, L., & Volk, H. 2003, A&A, 412, L11

Bret, A., Stockem, A., Fiuza, F., Ruyer, C., Gremillet, L., Narayan, R., & Silva, L. O., 2013, Physics of Plasmas, 20, 42102

Casse, F, Lemoine, M, & Pelletier, G. 2002, PhRvD, 65, 023002

Erlund, M., Fabian, A., Blundell, K., Crawford, C., & Hirst, P. 2010, MNRAS, 404, 629

Fanaroff, B., & Riley, J. 1974, MNRAS, 167, 31P

Gallant, Y. & Achterberg, A. 1999, ApJ, 305, L6

Giannios, D., & Spitkovsky, A. 2009, MNRAS, 400, 330

Godfrey, L., & Shabala, S. 2013, ApJ, 767, 12

Hardcastle, M., & Krause, M. 2014, MNRAS, 443, 1482

Hillas, A. 1984, ARA&A 1984, 425

Kirk, J., Guthmann, A., Gallant, Y., & Achterberg, A., 2000, ApJ, 542, 235

Lemoine, M., & Pelletier, G. 2010, MNRAS, 402, 321

Murase, K., Dermer, C., Takami, H. & Migliori, G. ApJ, 749, 63

Orienti, M., Prieto, M., Brunetti, G., et al. 2012, MNRAS, 419, 2338

Pelletier, G., Lemoine, M. & Marcowith, A. 2009, MNRAS, 393, 587

Reville, B., & Bell, A. 2014, MNRAS, 439, 2050

Schure, K., Bell, A., O'C Drury, L., & Bykov, A. 2012, Space Sci. Rev., 173, 491

Sironi, L., & Spitkovsky, A. 2011, ApJ, 726, 75

Sironi, L., Spitkovsky, A. & Arons, J. 2013, ApJ, 771, 54

Stage, M., Allen, G., Houck, J., & Davis, J. 2006, Nature Physics, 2, 614

Steenbrugge, K., & Blundell, K. 2008, MNRAS, 388, 1457

Vink, J., & Laming, J. 2003, ApJ, 584, 758

This 2-column preprint was prepared with the AAS LaTeX macros v5.2.